RL-TR-93-136
In-House Report
July 1993

# GIGAHERTZ OPTICAL LOCK-IN DEMULTIPLEXER

Jonathan Kane

DTIC
SELECTE
FEB 10 1995
S D
B

*APPROVED FOR PUBLIC RELEASE; DISTRIBUTION UNLIMITED.*

This effort was funded totally by the Laboratory Director's fund.

19950203 385

Rome Laboratory
Air Force Materiel Command
Griffiss Air Force Base, New York

This report has been reviewed by the Rome Laboratory Public Affairs Office (PA) and is releasable to the National Technical Information Service (NTIS). At NTIS it will be releasable to the general public, including foreign nations.

RL-TR-93-136 has been reviewed and is approved for publication.

APPROVED: Richard Payne

RICHARD PAYNE, Chief
Photonic Devices Technology Division
Electromagnetics and Reliability Directorate

FOR THE COMMANDER: Harold Roth

HAROLD ROTH
Director of Solid State Sciences
Electromagnetics and Reliability Directorate

If your address has changed or if you wish to be removed from the Rome Laboratory mailing list, or if the addressee is no longer employed by your organization, please notify RL( EROP ) Hanscom AFB MA 01731-5000. This will assist us in maintaining a current mailing list.

Do not return copies of this report unless contractual obligations or notices on a specific document require that it be returned.

# REPORT DOCUMENTATION PAGE

*Form Approved*
*OMB No. 0704-0188*

Public reporting for this collection of information is estimated to average 1 hour per response, including the time for reviewing instructions, searching existing data sources, gathering and maintaining the data needed, and completing and reviewing the collection of information. Send comments regarding this burden estimate or any other aspect of this collection of information, including suggestions for reducing this burden, to Washington Headquarters Services, Directorate for Information Operations and Reports, 1215 Jefferson Davis Highway, Suite 1204, Arlington, VA 22202-4302, and to the Office of Management and Budget, Paperwork Reduction Project (0704-0188), Washington, DC 20503.

| 1. AGENCY USE ONLY (Leave blank) | 2. REPORT DATE | 3. REPORT TYPE AND DATES COVERED |
|---|---|---|
| | July 1993 | IN-HOUSE |

**4. TITLE AND SUBTITLE**

GIGAHERTZ OPTICAL LOCK-IN DEMULTIPLEXER

**5. FUNDING NUMBERS**

PE: 61101F
PR: LDFP
TA: 02
WU: H2

**6. AUTHOR(S)**

JONATHAN KANE

**7. PERFORMING ORGANIZATION NAME(S) AND ADDRESS(ES)**

Rome Laboratory
80 Scott Road
Hanscom AFB, MA 01731-2909

**8. PERFORMING ORGANIZATION REPORT NUMBER**

RL-TR-93-136

**9. SPONSORING/MONITORING AGENCY NAME(S) AND ADDRESS(ES)**

**10. SPONSORING/MONITORING AGENCY REPORT NUMBER**

**11. SUPPLEMENTARY NOTES**

This effort was funded totally by the Laboratory Director's Fund.

**12a. DISTRIBUTION/AVAILABILITY STATEMENT**

APPROVED FOR PUBLIC RELEASE; DISTRIBUTION UNLIMITED

**12b. DISTRIBUTION CODE**

**13. ABSTRACT (Maximum 200 words)**

The primary goal of this effort was to investigate a new method of demultiplexing time varying optical images using a photorefractive optical mixer. The effort was based upon previous in-house work at Rome Laboratory with Jehad Khoury and Charles Woods. They demonstrated that the technique is valid for low frequencies (<100 Hz). The object of this research was to extend this concept to the range of GHz carrier frequencies. A second effort was to demonstrate that the concept could also be implemented with semiconductor lasers.

DTIC QUALITY INSPECTED 4

| 14. SUBJECT TERMS | 15. NUMBER OF PAGES |
|---|---|
| Demultiplexing, Optical lock-in, Semiconductor lasers, Photorefractives | 28 |
| | 16. PRICE CODE |

| 17. SECURITY CLASSIFICATION OF REPORT | 18. SECURITY CLASSIFICATION OF THIS PAGE | 19. SECURITY CLASSIFICATION OF ABSTRACT | 20. LIMITATION OF ABSTRACT |
|---|---|---|---|
| UNCLASSIFIED | UNCLASSIFIED | UNCLASSIFIED | UL |

# Contents




Accession For
NTIS GRA&I ☑
DTIC TAB ☐
Unannounced ☐
Justification
By
Distribution/
Availability Codes
Dist | Avail and/or Special
A-1

# Illustrations

# Tables

# Gigahertz Optical Lock-in Demultiplexer

## 1. INTRODUCTION

Photorefractive devices have attracted great interest recently. This report describes our investigation of a new method of demultiplexing time varying optical images using a photorefractive optical mixer. The effort was based on previous in-house work at the Rome Laboratory with Jehad Khoury and Charles Woods.[1] They demonstrated that the technique works at low frequencies (less than 100 Hz). Our investigation was designed to extend this concept to the range of GHz carrier frequencies.

A second effort sought to demonstrate that the concept could be implemented with semiconductor lasers.

Received for publication 13 July 1993

[1] Khoury, J., Kane, J.S., Keirstead, J., Woods, C., and Hemmer, P. (1994) Real-time holographic baseband frequency demodulator, (App. A) *Appl. Opt.* **33**(No. 14), 2909-2916.

## 2. LOW FREQUENCY IMAGE DEMULTIPLEXING

We investigated a new optical approach to frequency division demultiplexing that allows entire images to be demultiplexed in a single operation. This could allow massively parallel demultiplexing, which can be used to increase the channel capacity of a communication network. In our approach, images can be separated if their carrier frequencies exceed the inverse response time of the photorefractive medium (typically between 1 msec and 1 sec). This corresponds to a carrier frequency separation of a few hundred hertz as opposed to the several megahertz required for electronic demultiplexing of video information.

The basic architecture of an optical demultiplexer is shown in Figure 1. As in the electronic analog, several input images $O_1$ (x, y, t), $O_2$ (x, y, t)...$O_n$ (x, y, t) are generated in the first stage of the optical demultiplexer, which are individually phase modulated by sub-frequencies $f_1$, $f_2$....$f_n$ respectively. The modulated images are combined and transmitted to the receiver as the object beam of a photorefractive demultiplexer. The reference beam is generated separately with a modulation frequency, $f_r$, which can be tuned to any of the desired image modulation frequencies. Reference and object beams are then interfered in a photorefractive crystal to produce a real-time hologram. The different modulation frequencies present in the system produce running interference fringes that will result in the difference and summation frequencies ($f_1$-$f_r$, $f_2$-$f_r$.....$f_n$-$f_r$, $f_1$+$f_r$, $f_2$+$f_r$.....$f_n$+$f_r$) and their multiple integers. These moving fringe patterns will generate moving holographic gratings in the medium. However, for fast modulation frequencies, the finite response time of the material will lead to suppression of rapidly moving gratings. Thus, low pass filtering results and a backward read beam, $A_p$, will diffract off only those gratings that move slowly enough for the photorefractive media to respond. If the modulation frequency of the reference beam $f_r$ is equal to the modulation frequency for a particular image, then recovery of that image occurs via standard four-wave mixing phase conjunction.

The results from our experiment setup are shown in Figure 2. Figure 2A shows the output signal with no modulation present. This signal is two multiplexed images 01 and 02, shown in Figures 2B and 2C respectively. When both beams are phase modulated, both images disappear from the phase conjugate return as shown in Figure 2D. To recover 01, the reference beam is modulated to the same signature frequency (25 Hz). The resultant phase conjugate signal is shown in Figure 2E. As can be seen, image 01 is recovered without visible crosstalk. Similarly, modulating the reference beam at the signature frequency of 02 (200 Hz), allowed 02 to be recovered without visible crosstalk as shown in Figure 2F. Note the lack of any apparent degradation of the image resolution or signal to noise due to the demultiplexing operation.

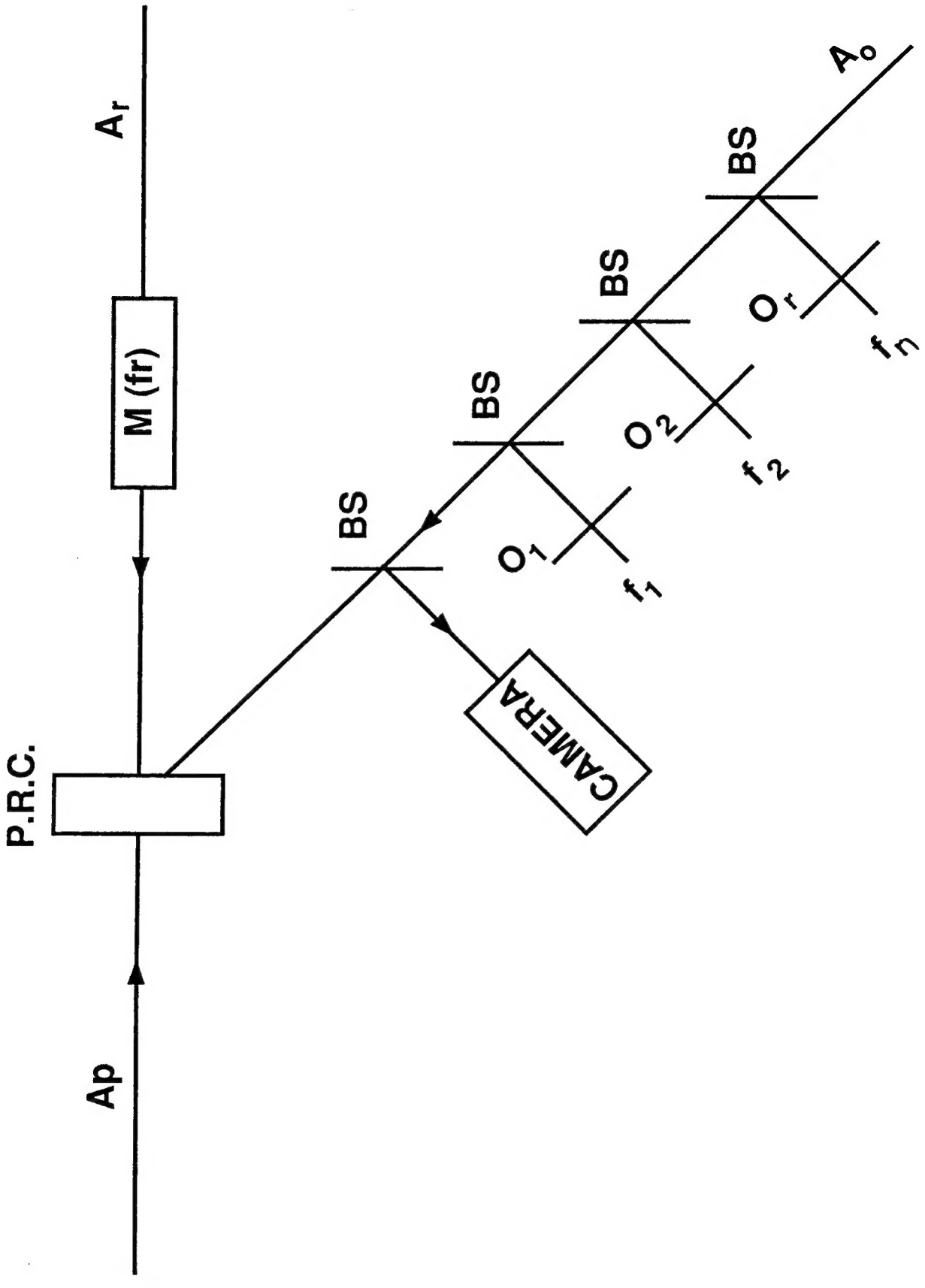


Figure 1. Basic Architecture of Photorefractive Demultiplexer.

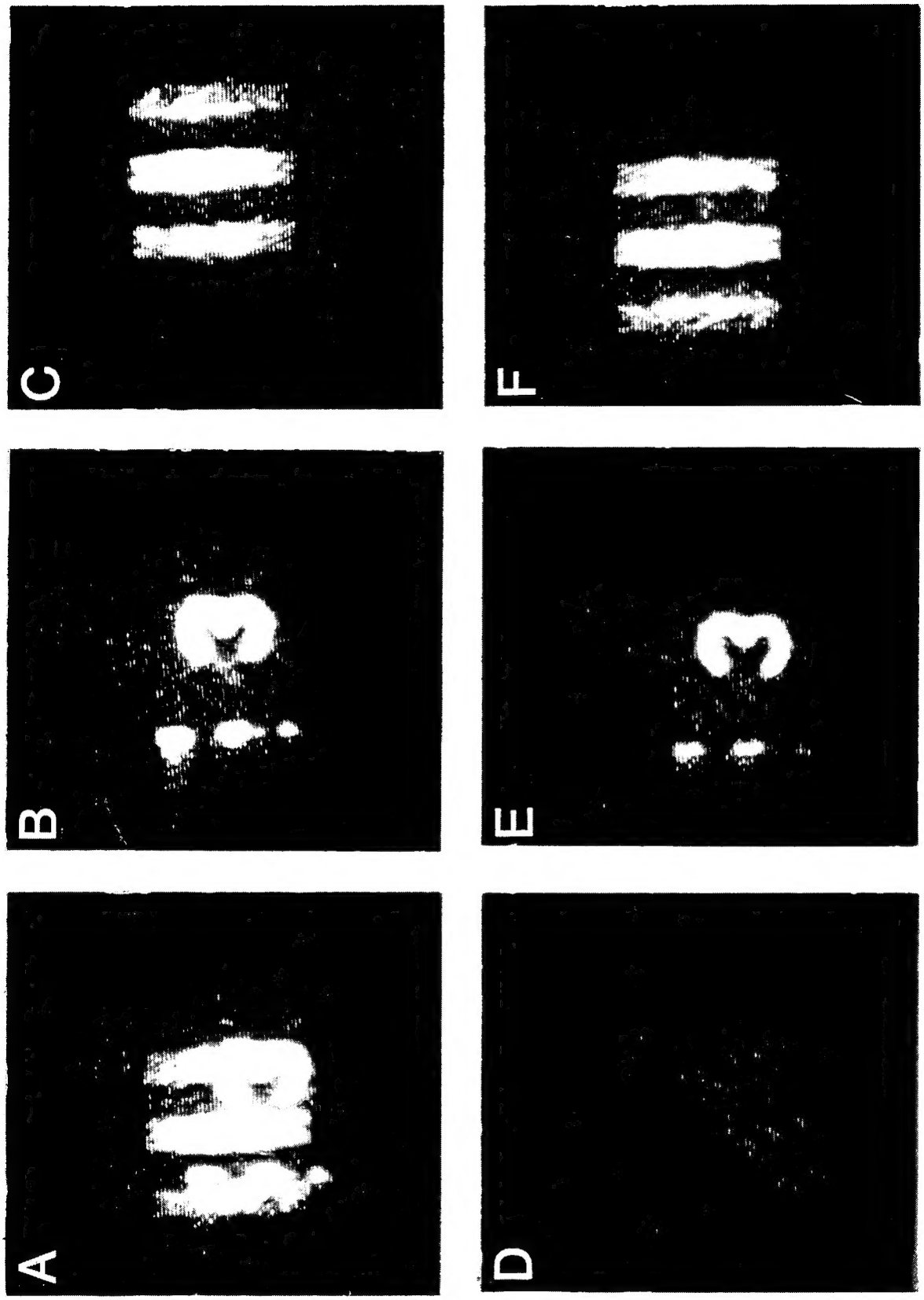


Figure 2: Experimental results of image demultiplexing. (A) Images O1 and O2 multiplexed together (no modulation) (B) Image O1 (C) Image O2 (D) Output of multiplexer in full modulation case (E) Recovery of image O1 via electronically locking the reference beam to the signature frequency associated with O1 (F) Recovery of O2.

## 3. GHz HETRODYNE DETECTION

For this demonstration experiment, the reference beam is modulated at 1 GHz. The object beam is then phase modulated with a second microwave signal, also near 1 GHz, but 0.8 Hz above the reference modulation frequency. This causes the output signal to reappear with an intensity that oscillates at the 0.8 Hz beat frequency. To record this beat signal, a photodiode was placed at the output plane and its signal is displayed on one channel of a chart recorder. The resulting data appears in the top traces of Figure 3, where the bottom traces display the amplitude of an electronic beat signal derived from a microwave mixer. The different data sets in Figure 3 correspond to different modulation amplitudes in the object beam. Figure 3A demonstrates the case of a small distorted sine wave where the minimum signal is zero within our 15 dB on/off ratio measurement. For larger phase modulation amplitudes in the object beam, as shown in Figures 3B and 3C, additional structure appears in the oscillating phase conjugate signal. Physically, this structure arises from holographic interference between the higher order phase modulation sidebands in both the reference and object beams. It should be noted that the modulation was provided by lithium tantalate modulators designed and constructed in-house.

We also tried using carrier frequency differences larger than 0.8 Hz and found that the phase conjugate signal is attenuated more than a factor of 10 for beat signals greater than about 30 Hz. Since similar results were previously observed at sub-kHz carrier frequencies (see Appendix, Reference 6) we can infer that our demonstrated image demultiplexing technique can also be extended to 1 GHz carrier frequencies.

## 4. LASER DIODE EXPERIMENTS

The next phase in the initiative was to show that the technique could be extended to an all solid-state device. We spent several months experimenting with different diode lasers and crystals, trying to find the right crystal/diode laser combination to achieve phase conjugation. The problem is that most of the photorefractive devices operate in the 400-600 nanometer range whereas most of the diode lasers operate in the 700-1000 nanometer range. Eventually we successfully produced a phase conjugator with an 850 nanometer diode laser and a high-resistivity p-type undoped GaP crystal.

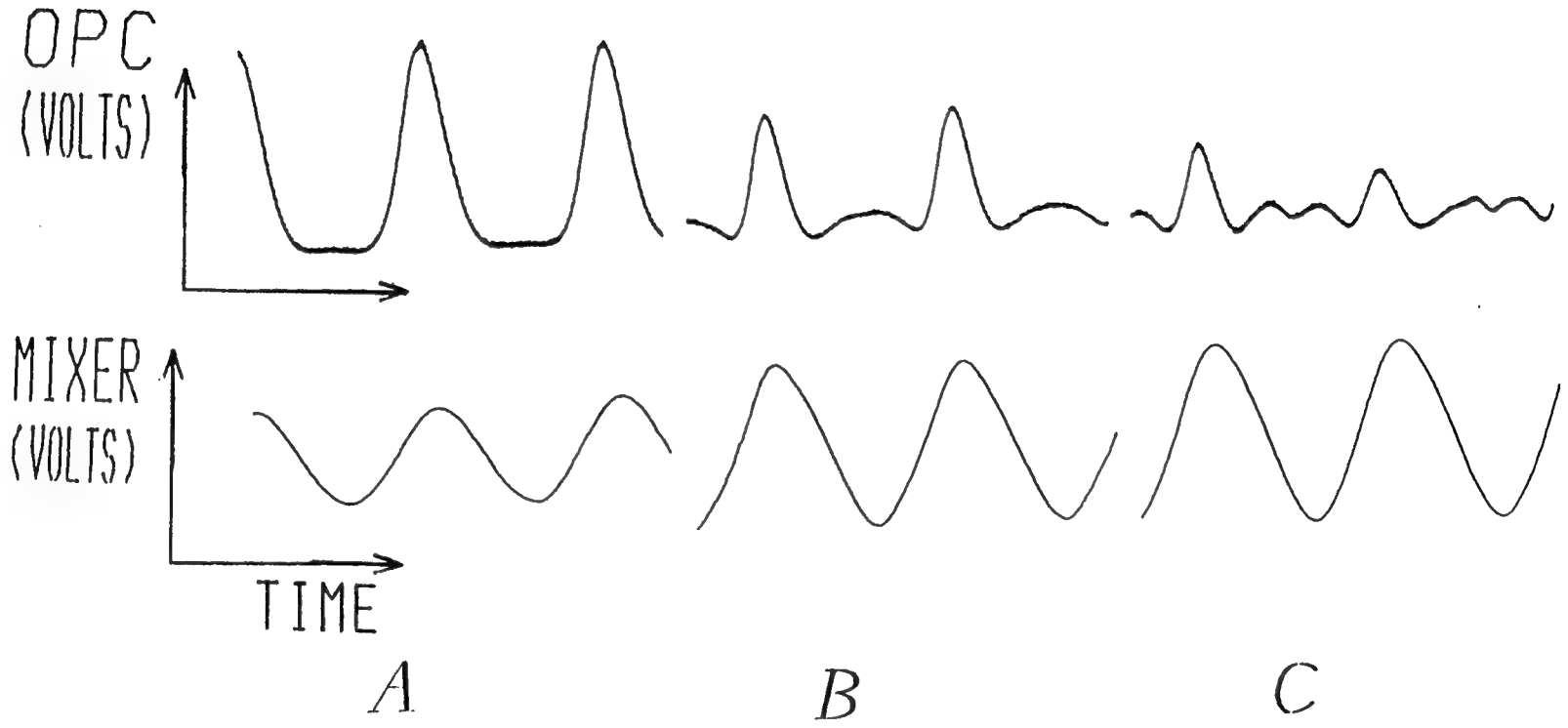


Figure 3. Phase Conjugate Output Signal (Top Trace) and Microwave Mixer Output (Bottom Trace) vs Time. (A) Low modulation amplitude. (B) Larger modulation amplitude. (C) Maximum modulation amplitude.

In the experiment we demonstrated phase sensitive detection by amplitude modulating the laser directly at up to 7 GHz and varying the path length of the object beam. Table 1 summarizes the results. The phase conjugate is brightest when the two beams are in phase with each other which occurs periodically with modulation wavelength, as expected. A photograph of the experimental setup is provided in Figure 4.

Table 1. Measurements of Peak Output Response in Terms of Path Difference. Column 1 is the modulation frequency of the laser diode. Column 2 is the corresponding modulation wavelength. Columns 3, 4, and 5 indicate the amount of path difference between consecutive output peaks. Note that the peaks repeat periodically.

| Frequency of Modulation (Ghz) | Calculated Path Difference (cm) | Measured Path Difference (cm) | | |
|---|---|---|---|---|
| | | 1 | 2 | 3 |
| 3 | 10.0 | 0 | 10.0 | n.a. |
| 4 | 7.5 | 0 | 7.0 | 15.0 |
| 5 | 6.0 | 0 | 6.0 | 12.0 |
| 6 | 5.0 | 0 | 5.0 | 10.0 |
| 6.8 | 4.4 | 0 | 4.2 | 8.8 |

## 5. DYNAMIC VIDEO IMAGE DEMULTIPLEXING

In a final series of experiments we tried to demonstrate the demultiplexing technique with dynamic video imagery. Video image demultiplexing in our setup was more complicated, because the modulator we had available was a liquid crystal television, which introduced enough absorption and phase aberration to put us close to the level of minimum detection. We were able to demultiplex the imagery; the poor image quality does not reproduce well. For completeness we have included two successive frames from our videotape (see Figures 5A and 5B) which show two successive frames when the reference and object beam were electronically phase locked. Note in Figure 5B that there is a bright spot in the center which is not in Figure 5A. We hope to improve the results when a better spatial light modulator becomes available.

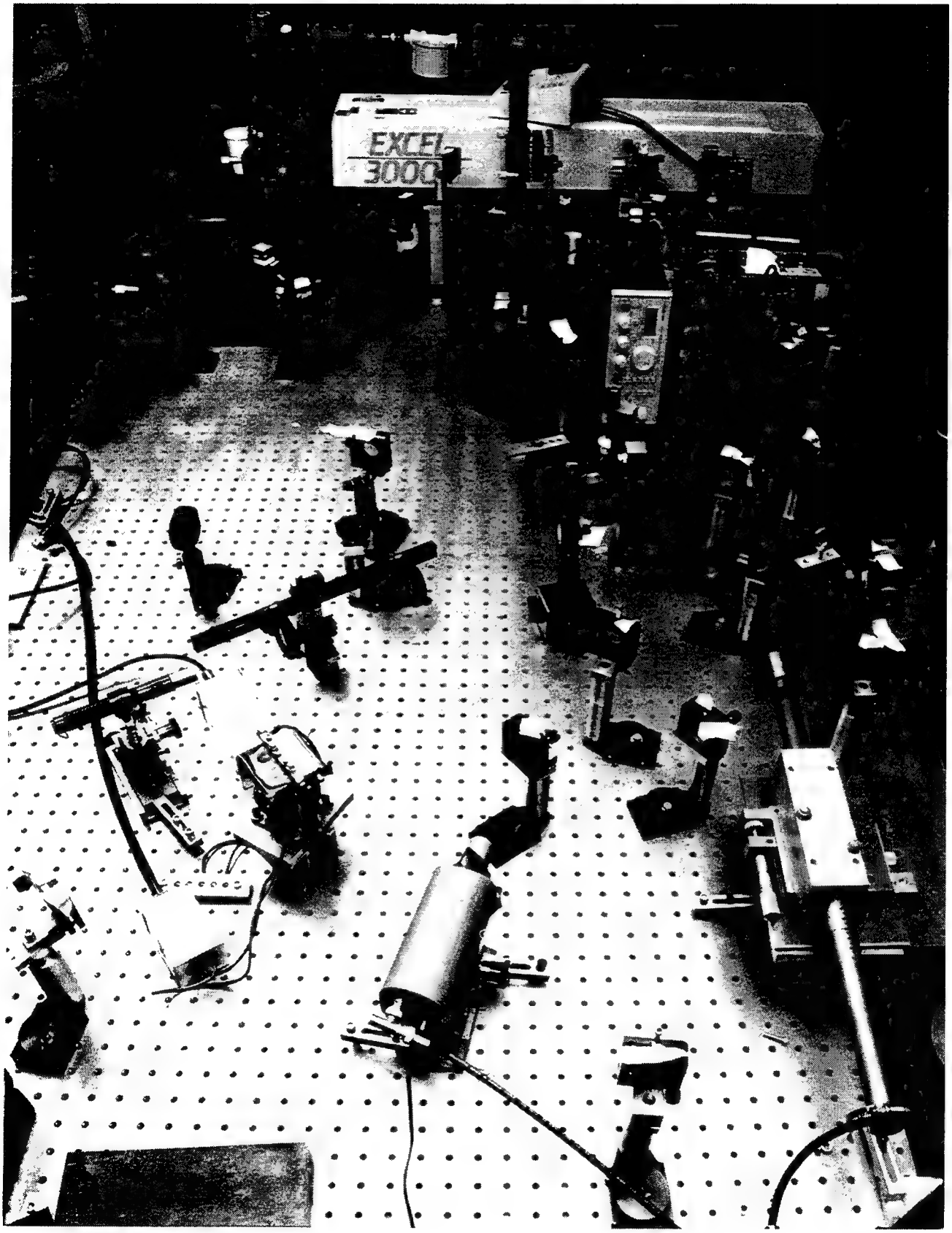


Figure 4 : Photograph of laser diode experimental setup.

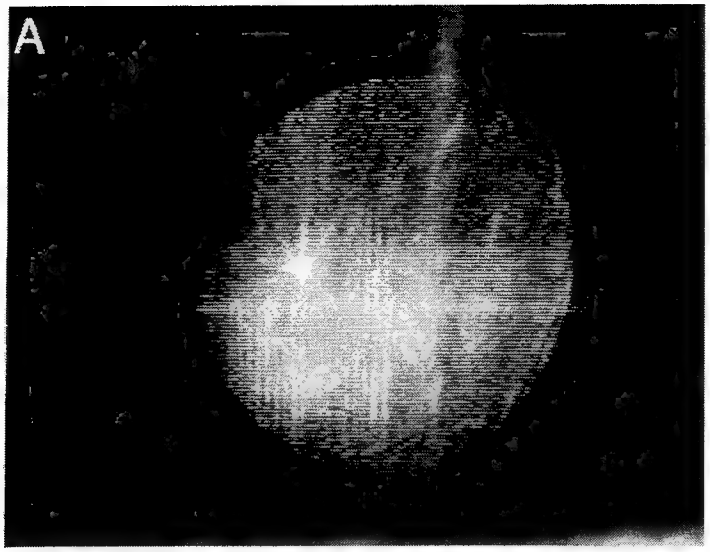


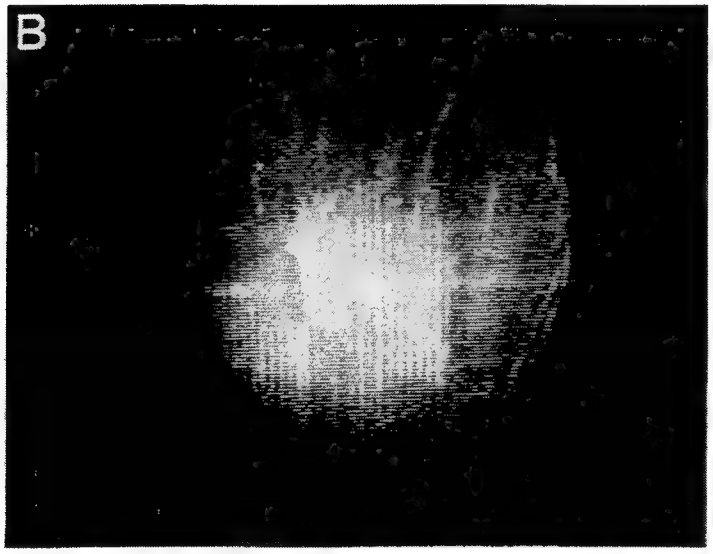


Figure 5 : Two successive frames of the demodulator output when a LCTV was used to produce a video output. Note that in (B) there is a bright spot in the center which does not exist in (A).

## 6. SUMMARY

In this research initiative we have successfully demonstrated a novel photorefractive optical demultiplexer. We have shown that the techniques can be applied to demultiplexing video images and is extendable to GHz frequencies. In addition we have demonstrated that the technique can be eventually transferred over to industrial applications via an all solid-state device.

We have published one paper in Applied Optics, Real-time holographic baseband frequency demodulator, by Khoury, Kane, Kierstead, Woods, and Hemmer, and are currently preparing one more entitled "Frequency classifier" which discusses several other methods of implementing the photorefractive device based upon the theory developed above.

## References

1. Khoury, J., Kane, J.S., Keirstead, J., Woods, C., and Hemmer, P. (1994) Real-time holographic baseband frequency demodulator, (App. A), *Appl. Opt.* **33**(No. 14), 2909-2916.

# Appendix A

# Real-Time Holographic Baseband Frequency Demodulator

The U.S. Government is authorized to reproduce and sell this report. Permission for further reproduction by others must be obtained from the copyright owner.

a reprint from Applied Optics

# Real-time holographic baseband frequency demodulator

Jehad Khoury, Jonathan S. Kane, John Kierstead, Charles Woods, and Philip Hemmer

The multiplicative and low-bandpass filtering characteristics of real-time holograms in photorefractive media are used as a basis for a baseband frequency demodulator by means of holographic homodyne detection. We experimentally demonstrate the demodulation of spatial bandpass signals in the kilohertz regime and homodyne detection in the gigahertz regime.

## Introduction

Hetrodyne interferometry[1] and time-integrative processing[2] have become areas of great interest in the optical signal-processing community. Most of the devices used for this purpose such as CCD cameras or spatial light modulators[3,4] use active elements for time integration. It was recently demonstrated that real-time holographic materials can also be used as time-integrative devices.[5–7] In this paper we present an optical approach to frequency baseband demodulation that uses a photorefractive crystal. The technique has several advantages over the approach outlined by Takeda and Kitoh[1]: first, our device does not require phase objects; second, three-dimensional holograms can be demultiplexed; third, the demodulator is a phase conjugator that also has the ability of real-time aberration correction and dispersion correction[8]; fourth, it is an all-optical device that permits cascading for purposes of optical computing; and fifth, our device works from kilohertz modulation frequencies all the way to gigahertz frequencies. To our knowledge, no other single device has all of these combined features.

In this paper we experimentally demonstrate theoretical research on image demodulation by using a photorefractive crystal (at subkilohertz carrier frequencies), and we also extend the homodyne and heterodyne detection capability[6] out to a carrier frequency of 1 GHz.

## Theory

The basic architecture of an optical demodulator is shown in Fig. 1. As in the electronic analog, the first stage of the optical demodulator involves generating several input images $O_1(x, y, t)$, $O_2(x, y, t), \ldots,$ $O_n(x, y, t)$, which are individually phase modulated by subfrequencies $f_1, f_2, \ldots, f_n$, respectively. The modulated images are combined and transmitted to the receiver as the object beam of a photorefractive demodulator. The reference beam is generated separately with a modulation frequency $f_r$, which can be tuned to any of the desired image-modulation frequencies. We then interfere reference and object beams in a photorefractive crystal to produce a real-time hologram.

For static images, the different modulation frequencies present in the system produce running interference fringes that will result in the difference and summation frequencies (i.e., $f_1 - f_r, f_2 - f_r, \ldots, f_n - f_r$; $f_1 + f_r, f_2 + f_r, \ldots, f_n + f_r$) and their multiple integers. These moving fringe patterns will generate moving holographic gratings in the medium. However, for fast modulation frequencies, the finite response time of the material will lead to the suppression of rapidly moving gratings. Thus low-pass filtering results, and a backward read beam $A_p$ will only diffract off of those gratings that move slowly enough for the photorefractive media to respond. If the modulation frequency of the reference beam $f_r$ is equal to the modulation frequency for a particular image, then recovery of that image occurs by means of a standard four-wave mixing phase conjugation. Because a standard four-wave mixing setup is used, the resolution achievable with this demultiplexing scheme is high (of the order of 1000 lines/mm for BSO crystal).

J. Khoury is with Tufts University, Medford, Massachusetts 02155; J. S. Kane, C. Woods, and P. Hemmer are with the Optical Signal Processing Branch, Rome Laboratory, Hanscom Air Force Base, Massachusetts 01731; J. Kierstead is with Parke Mathematical Laboratories, Bedford, Massachusetts 01731.

Received 15 April 1993; revised manuscript received 25 October 1993.

0003-6935/94/142909-08$06.00/0.

© 1994 Optical Society of America.

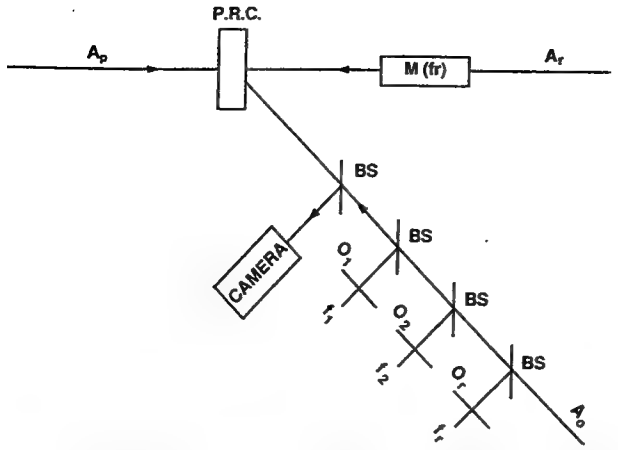


Fig. 1. Conceptual setup for real-time holographic baseband frequency demodulator. Each object beam with its own signature frequency is multiplexed onto a single laser beam. To demultiplex any of the given object beams, we electronically lock the reference-beam modulator to the desired signature frequency. The given object is recovered at the camera. P.R.C., photorefractive crystal; M(fr), modulation frequency; BS's, beam splitters.

The case of demodulating video images is related to baseband transmission. In this discussion we give the final result without giving all the theoretical details. A more detailed explanation is currently under review for publication.[9]

In the case of lock-in of the $i$th object, the result of the space-charge field is given by

$$E_{sci}(x, y, t) \propto \int_{-\infty}^{+\infty} \left[\frac{O_i(x, y, \omega)}{-i\omega\tau + 1} \exp(i\omega\tau)\mathrm{d}\omega\right] E_{scpl}(\phi), \quad (1)$$

where

$$O_i(x, y, \omega) = \int_{-\infty}^{+\infty} O_i(x, y, t)\exp(-i\omega t)\mathrm{d}t, \quad (2)$$

where $E_{scpl}$ is the space-charge field of the phase locking between the reference beam and the $i$th object beam. For example, the space-charge field of the phase locking between two sine phase-modulated beams is given by

$$E_{scpl} = \frac{GA_1A_2}{I_o} \sum_{n=-\infty}^{\infty} J_n(\delta_1)J_n(\delta_2)\exp(in\phi), \quad (3)$$

where $\delta_1$ and $\delta_2$ are the amplitudes of the phase modulation of the two interfering beams,[6] $A_1$ and $A_2$ are the fields of the interfering beams on the crystal, $I_o$ is the average intensity incident on the crystal, $J_n$ is the $n$th-order Bessel function, $\phi$ is the phase difference between the modulating inputs, and $G$ is a factor proportional to the coupling coefficient.

If we assume that the material has a fast enough response time, such that $\omega\tau \ll 1$ where $\tau$ is the response time of the photorefractive material, then

$$E_{sci}(x, y, t) \propto O_i(x, y, t)E_{scpl}(\phi), \quad (4)$$

and recovery of the $i$th image occurs.

## Experimental

Our experimental setup for demonstrating optical image demultiplexing is illustrated in Fig. 2. As shown in the figure, an argon laser is divided into several beams: a reference beam $A_r$, two diverging object beams, and a readout beam $A_p$. The intensities of each beam are 10 mW for $A_r$, 2.0 mW for the object beam passing through object $O_1$, 1.6 mW for the beam passing through object $O_2$, and 14 mW for the read beam $A_p$. The spot diameters for all beams are approximately 2 mm at the surface of the crystal. However, the spot sizes of the diverging object beams before $O_1$ and $O_2$ were approximately 1 cm. Each object beam also passes through its respective choppers $C_1$ and $C_2$ to generate the baseband signal on the spatial information. We combine the two object beams and make them approximately collinear in order to generate the signal beam as shown in the figure. The signal beam is then interfered with the reference beam in the BSO crystal. The resulting hologram is read out by means of $A_p$. We controlled the polarization of $A_p$ by a quarter-wave plate to separate the output from the scattered light from the crystal surface.

The phase modulation is provided by means of piezoelectric mirrors $PZM_1$, $PZM_2$, and $PZM_3$ in each of beams $A_1$, $A_2$, and $A_r$, respectively. The baseband signal was introduced through rotating choppers $C_1$ and $C_2$, which rotated at 66 and 50 Hz, respectively. We transfer static information to each object beam by placing separate transmissive resolution charts $O_1$ and $O_2$ in the respective object beam paths.

Figure 3(a) shows the phase-conjugative output signal with no modulation present. This signal is the summation of the demodulated inputs $O_1$ and $O_2$ shown in Figs. 3(c) and 3(d), respectively. When

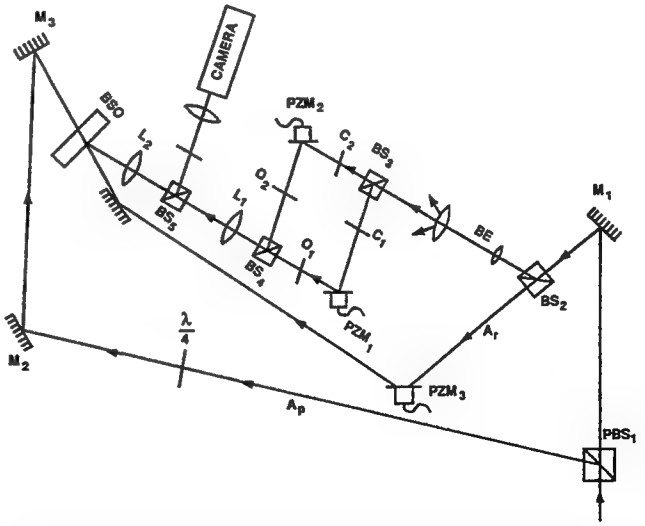


Fig. 2. Experimental setup for optical demultiplexing (see text). The modulation of the beams is accomplished through piezoelectric transducers $PZM_1$–$PZM_3$. The baseband signal is generated by choppers $C_1$ and $C_2$. O's, transmissive objects; M's, mirrors; L's, lenses; BS's, beam splitters; BE, beam expander; $PBS_1$, polarizing beam splitter; $\lambda/4$, quarter-wave plate.

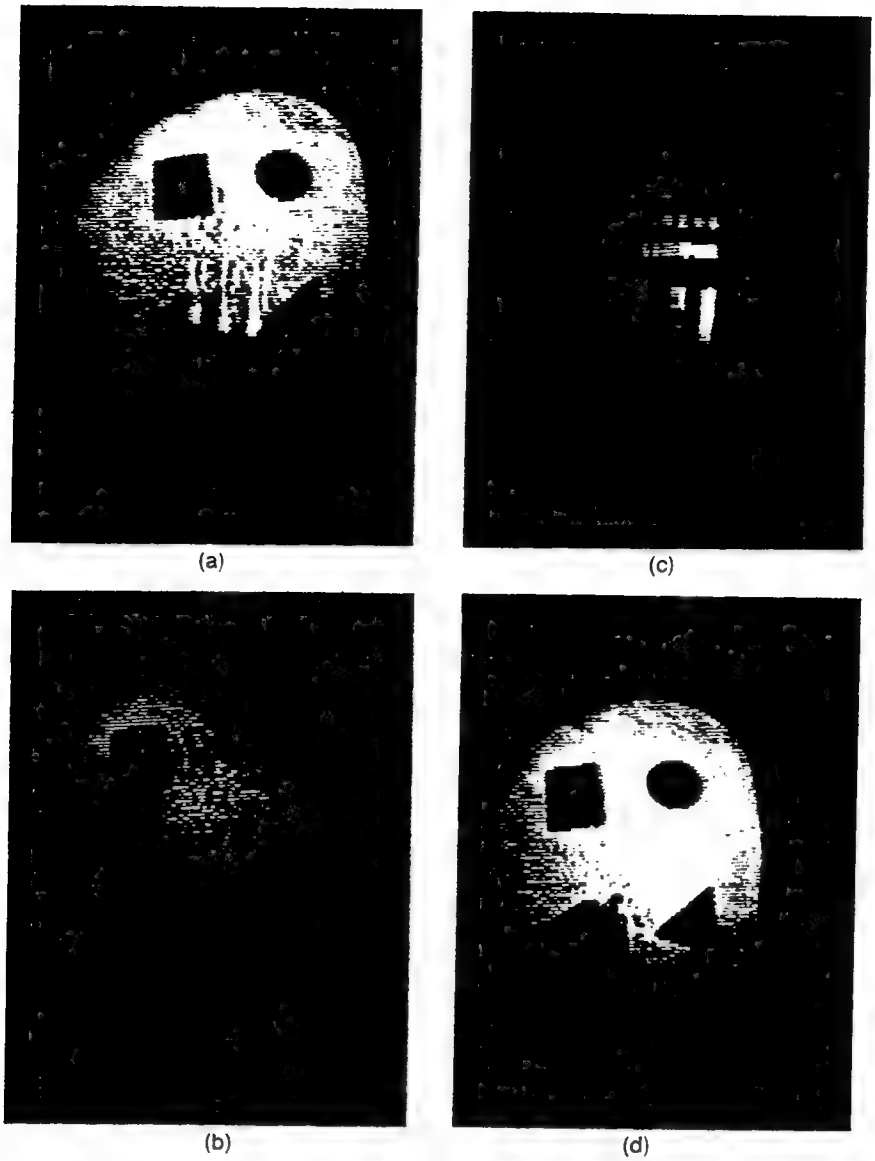


Fig. 3. Output of frequency demodulator: (a) summation of $O_1$ and $O_2$ (no modulation), (b) modulated output beam, (c) recovery of $O_1$ when electronically phase locked to reference beam, (d) recovery of $O_2$ when electronically phase locked to reference beam.

$PZM_1$ and $PZM_2$ phase modulate their respective object beams, both images almost disappear from the phase-conjugate return as shown in Fig. 3(b). The phase modulation utilized in this case was provided by a piezoelectric transducer driven by a sine-wave voltage with a modulation amplitude of 10.8 rad peak to peak. In order to get the phase conjugate to disappear completely, we need a slightly higher voltage than our modulators can provide.

To recover $O_1$, we modulate the reference beam at the same frequency as that of $A_1$ (660 Hz). The resultant phase-conjugate signal is shown in Fig. 3(c). As we can see, image $O_1$ is recovered with little cross talk. Similarly, modulating the reference beam at the same frequency as that of $A_2$ (3 kHz) permitted $O_2$ to be recovered with little cross talk , as shown in Fig. 3(d).

Note that Figs. 3(c) and 3(d) represent the results when the phase modulations in the reference and signal beams are electronically in phase and the choppers only partially obscure the images. When the phase locking is not exactly in phase we observe darker recovered images, as we quantitatively illustrate in the next section.

### Baseband Transmission

To measure quantitatively the demodulation of the transient signal, we removed $O_1$ and $O_2$, replaced the camera by a detector, and detected the output by electronically locking the modulation frequency of channel 1 or channel 2 to that of the reference modulation frequency. The phase modulation of the object piezoelectric transducers was sine-phase modulation adjusted to be approximately 10.8 rad peak to peak, so that any phase modulation was almost capable of erasing its respective grating in the BSO crystal. This phenomenon will occur as long as the modulation is fast in comparison with the response time of the crystal. However, the frequency modula-

tions of choppers $C_1$ and $C_2$ were within the bandwidth of the crystal.

Figures 4A and 4B show the result of baseband transmission for channel 1 and channel 2, respectively. In both figures there are three traces: the first for zero phase difference, the second for 22°, and the third for 45°. The relative ratios of beam intensities are given by 2.0, 1.0, and 0.3, which are in close agreement with the relative values for $E_{scpl}$ at the same corresponding angle of phase difference $\phi$ [see eq. (3)]. The relative theoretical values of $E_{scpl}$ are 2.0, 1.0, and 0.1. The discrepancy between experiment and theory is due to mutual erasure between the two channels. Note that the theoretical values were extracted from the plot $E_{scpl}$ as a function of $\phi$ when the modulation is sine-phase modulation with a peak-to-peak value of 1.6 $\pi$. This plot is shown in Fig. 5. These results validate relation (1) for image demodulation by using a low-coupling photorefractive crystal.

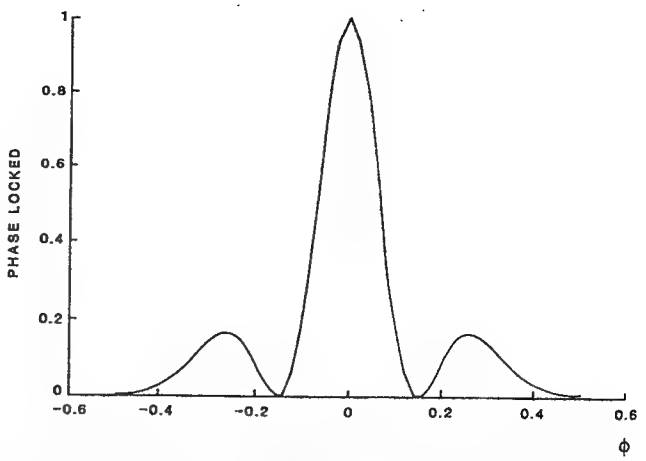


Fig. 5. Theoretical plot of space-charge field of the phase locking versus phase difference [see Eq. (3)].

### Video-Image Demultiplexing

Video-image demultiplexing in our setup was complicated to realize because our laser was low intensity (25 mW) and because the spatial light modulator was a liquid-crystal television (LCTV) that introduced enough absorption so that we were close to the level of minimum detection. To overcome these problems we only used one channel. To do so, we replaced beam splitter $BS_2$ in Fig. 2 by a variable neutral-density filter, we removed beam splitter $BS_3$, and we replaced beam splitter $BS_4$ with a mirror. We replaced $C_2$ and $O_2$ with a LCTV spatial light modulator. $PZM_2$ and $PZM_3$ were modulated at the same frequency but with different amplitudes of modulation as a way to ensure time-integrative behavior. Figures 6(a) and 6(b) show two successive frames in which the reference and object beam were electronically phase locked. We hope to achieve better results when a higher-power laser becomes available.

Thus far we have shown experimentally that two images can be demultiplexed with little cross talk for carrier frequencies in the subkilohertz range and for carrier-frequency separations of less than 200 Hz. Of course for a high-capacity demodulator this same performance must be demonstrated at much higher carrier frequencies.

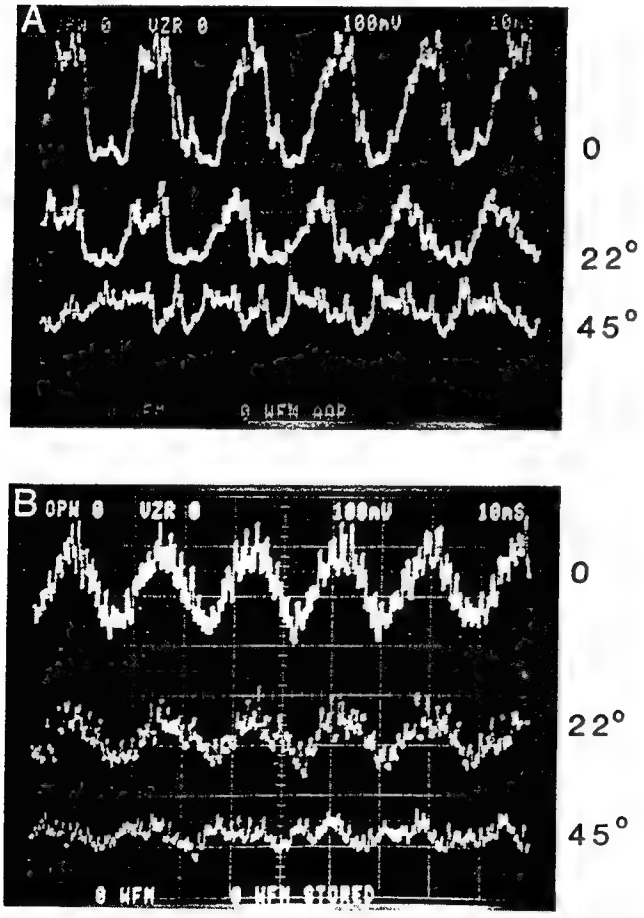


Fig. 4. Frequency demodulator output on photodetector (no images) with rotating chopper: Outputs of A, channel 1, and B, channel 2, when they are phase locked to the reference beam. The top trace is in phase, and the second and third traces are 22° and 45° phase lag, respectively.

### Gigahertz Heterodyne Detection

In theory, the maximum carrier frequencies are only limited by the optical frequency ($\cong 10^{15}$ Hz) subject to the geometric constraints required by holographic approaches. However, to approach this limit we would need separate reference and object lasers, and the effects of laser jitter would make implementation impractical. Instead, utilizing a high-speed (1-GHz) phase modulator, we can generate the necessary multiple optical frequencies by using a single laser so that absolute laser jitter becomes much less important. Unfortunately, only two high-speed modulators and microwave drivers were available to use for this experiment. Therefore, we are able to demonstrate the extension of the homodyne and heterodyne capability only out to 1-GHz carrier frequencies (using a single Gaussian object beam rather than two distinct images).

(a)

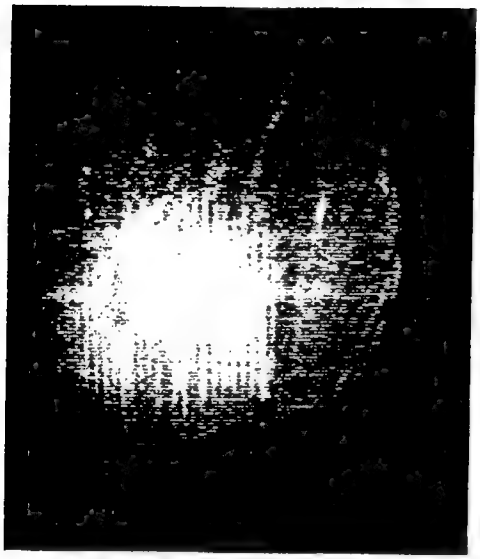

(b)

Fig. 6. (a), (b) Two successive frames of the demodulator output when a LCTV was used to produce a video output.

Figure 7 shows our modified experimental arrangement for 1-GHz homodyne detection. Once again, it is a standard four-wave mixing configuration that uses a bismuth silicon oxide (BSO) crystal and an intersection angle of 30° between reference and object wave. A He–Ne laser beam (2 mm in diameter) is divided into a reference beam R, an object beam O, and a readout beam B, with respective intensities of 2.2 mW, 3.8 mW, and 8 mW. As shown, we use $LiTaO_3$ electro-optic modulators to generate the 1-GHz phase modulation. These modulators are driven with independently synthesized microwave signals near 1 GHz, derived from a common quartz crystal. To achieve high drive voltages with less than 1 W of microwave input power, we mount the modulators in a resonant *LC* circuit (not shown) with a *Q* value of approximately 200 at 1 GHz. Crystal dimensions are 1 mm × 1 mm × 70 mm. Because

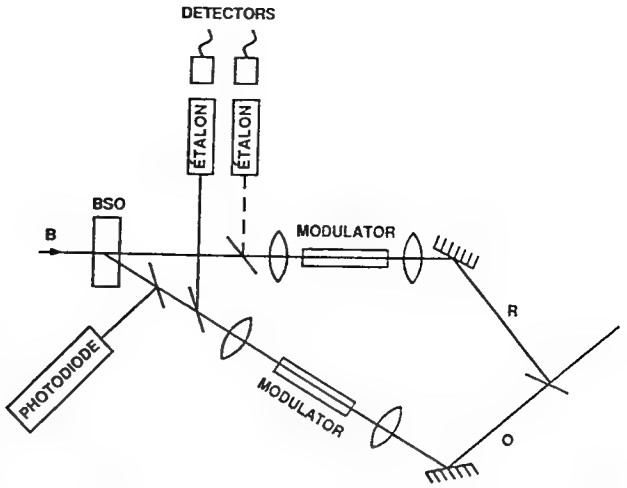


Fig. 7. Experimental setup for the demonstration of homodyne detection at 1 Ghz.

the input laser beams are too large to fit directly into the modulating crystals, telescopic arrangements with unity magnification are utilized as shown in Fig. 7. These telescopic arrangements consists of two 10-cm lenses, spaced 2 focal lengths apart with a modulator positioned at the beam waist.

To monitor the performance of the phase modulators, we pick off a portion of each modulated beam by a separate beam splitter and direct it to a Fabry–Perot étalon, as shown in Fig. 7. Figure 8 shows typical Fabry–Perot traces for the reference beam, where the Fabry–Perot has a free spectral range of approximately 4.5 GHz. Specifically, Fig. 8A corresponds to the case of no modulation. The broad (≅ 1-GHz-wide) Fabry–Perot resonances observed are a consequence of the multilongitudinal mode operation of the high-power He–Ne laser. Clearly independent lasers with such broad linewidths would not be practical for this type of demultiplexing operation.

Introducing a weak modulation voltage at 1 GHz into the reference-beam phase modulator generates the first-order sidebands, as shown in Fig. 8B. When the applied microwave power is increased (see Fig. 8C), strong suppression of the carrier results. Strong suppression of the carrier is important for reducing cross talk in a demultiplexing operation.

We now demonstrate homodyne detection that uses 1-GHz carrier frequencies as follows. The system is first aligned for maximum phase-conjugate return with both modulators off. Next the reference beam only is phase modulated at a frequency of approximately 1 GHz, where the modulation amplitude is large enough to suppress the carrier strongly (see Fig. 8C). At this point the conjugate signal vanishes. The measured on–off ratio for the phase-conjugate signal is greater than 15 dB where the measurement was limited by noise from the scattered light. The object beam is then phase modulated with a second microwave signal, also near 1 GHz but 0.8 Hz above the reference modulation frequency. This causes the phase-conjugate signal to reappear with an intensity that oscillates at the 0.8-Hz beat frequency. To

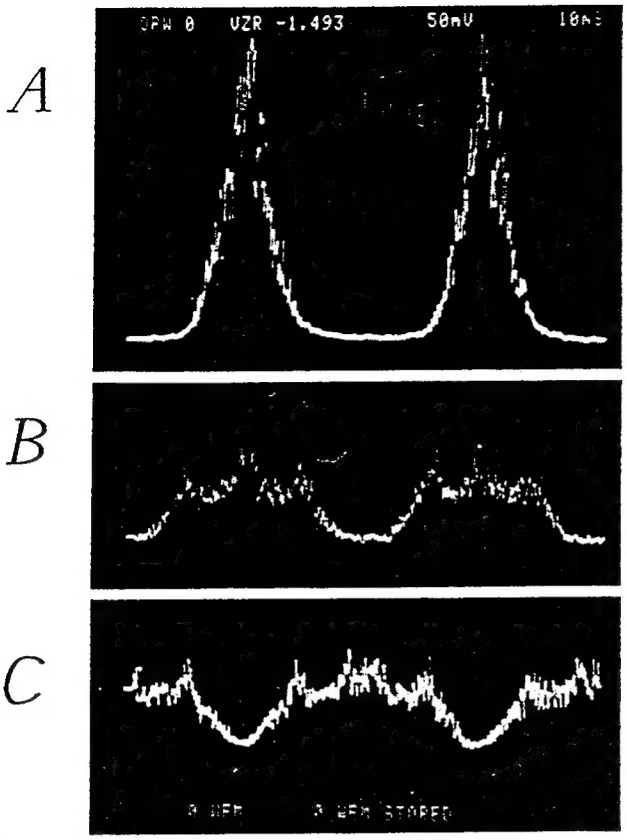


Fig. 8. Typical oscilloscope traces showing Fabry–Perot transmission for different modulation amplitudes: A, no modulation, broad resonances caused by the He–Ne laser linewidth; B, small modulation amplitude; C, large modulation amplitude, fundamental frequency disappears.

record this beat signal we place a photodiode at the output plane (see Fig. 7), and its signal is displayed on one channel of a chart recorder. The resulting data appear in the top trace of Fig. 9; the bottom trace displays the amplitude of an electronic beat signal derived from a microwave mixer.

The different data sets in Fig. 9 correspond to different modulation amplitudes in the object beam. Figure 9A demonstrates the case of a small modulation amplitude. As we can see, the phase-conjugate signal appears as a distorted sine wave in which the minimum signal is zero within the 15-dB on–off ratio measurement limitation mentioned above. For larger phase-modulation amplitudes in the object beam, as shown in Fig. 9B and 9C, additional structure appears in the oscillating phase- conjugate signal. Physically, this structure arises from holographic interference between the higher-order phase-modulation sidebands in both the reference and object beams (see Fig. 8C).

We also tried using carrier-frequency differences larger than 0.8 Hz, and we found that the phase-conjugate signal is attenuated more than a factor of 10 for beat signals greater than approximately 30 Hz. Similar results were previously observed at sub-kilohertz carrier frequencies.[6] From this we can infer that our demonstrated static image demultiplexing technique can also be extended to 1-GHz carrier frequencies.

Finally, we also examined the optical mixing and heterodyne capability of this technique by applying identical (1-GHz) phase modulation to both the object and reference beams. Figure 10 shows the resulting phase-conjugate and microwave mixer signals. In particular, when weak object beam modulation is employed (Fig. 10A) and several fixed phases are used, the optical phase conjugate follows the microwave phase difference approximately linearly. However, when higher modulation amplitudes are used (see Fig. 10B), the phase-conjugate intensity dependence on phase difference becomes clearly nonlinear.

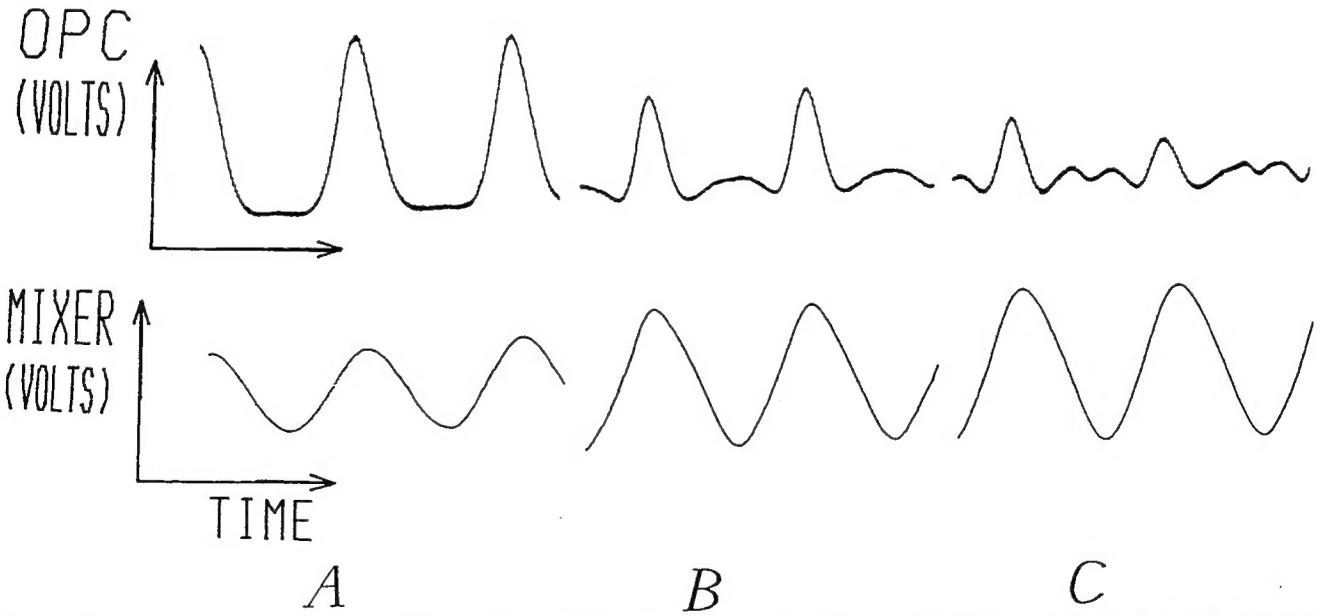


Fig. 9. Phase-conjugate output signal (OPC, top trace) and microwave mixer output (bottom trace) versus time: A, low modulation amplitude; B, larger modulation amplitude; C, maximum modulation amplitude.

## Discussion

Here we concentrate on two topics: image demultiplexing limits and the transmission of images with no available reference.

### Image Demultiplexing Limits

The number of images that can be demultiplexed is limited by the diffraction efficiency of the material. For example, if we use a BSO crystal, the number of images that can be demultiplexed will never realistically exceed a few images in the best case, because the diffraction efficiency will fall off approximately as $1/N^2$. For ten images the reduction in efficiency for every object is $10E + 2$. Most BSO crystals have efficiencies of $10E - 3$. Therefore, for ten objects the efficiency will drop to $10E - 5$, which is almost the limitation in current detection systems. However, as a result of the discovery of new crystals of barium titanate that have response times of 20 ms and typical coupling coefficients of $\gamma = 38.7\ \text{cm}^{-1}$,[10] time demultiplexing of 100 video images may be feasible.

The use of a material such as barium titanate, however, introduces another limitation because of second-order nonlinearities. This effect can be explained as follows. Assuming that all of our objects are simple beams (instead of complex patterns) and assuming that the device is locked to the $i$th beam, we find that a grating is written between the reference beam and the $i$th beam. This grating will scatter all the other beams in a direction colinear with the reference beam. The result is that the other beams will write a new grating with their respective scatter in the direction of the reference-beam grating. For static inputs, these new gratings will interfere constructively among themselves as well as with the locked grating.

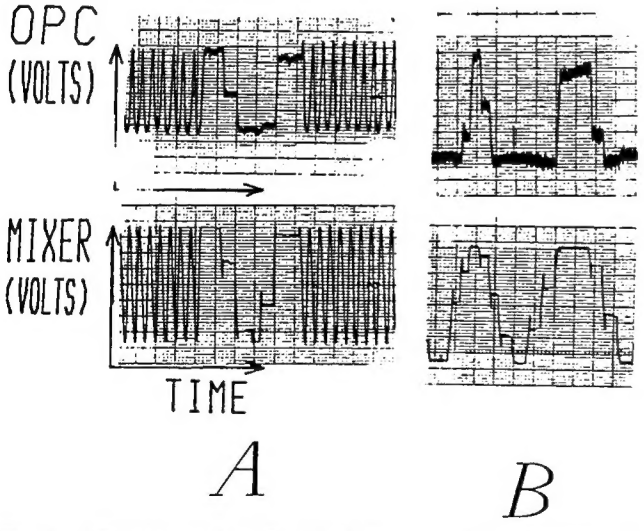


Fig. 10. Demonstration of optical phase-sensitive detection at 1-GHz carrier frequency. The top trace is the phase-conjugate output signal (OPC, from photodiode). The bottom trace is the electronic microwave mixer output. The phase is adjusted manually by the momentary change of the frequency of one microwave synthesizer. A, Low modulation. Note that the OPC follows the microwave mixer almost linearly. B, High modulation. Note that the OPC follows the microwave mixer nonlinearly.

The first-order grating will contribute to the original signal; however, all the high-order gratings will contribute to the modified signal. Our calculations of the efficiency after correction for the higher-order gratings can be summarized as[9]:

$$\eta = \frac{\eta_1}{1 - 0.5\gamma l \sum_{j=1}^{n} |O_j|^2 / I_o},$$

where $\eta_1$ is the amplitude efficiency of locking to a specific channel and $\eta$ is the corrected efficiency from high-order grating coupling. The derivations of this equation are beyond the scope of this paper and have been considered in another paper currently under review. For a large number of channels, note that $\Sigma|O_j|^2 \approx I_o$; therefore the modified signal is an enhanced version of the original signal. We have experimentally examined the cross talk by using a BSO crystal as well as a $BaTiO_3$ crystal in the low-coupling limit, and we have not observed any cross talk between the two channels caused by this effect.

### Image Recovery without a Known Reference Frequency

Image recovery without a reference frequency is also a possibility. For static images this can be done simply by tuning the reference modulation frequency near that of the object beam to be recovered. In this case, an oscillating phase-conjugate image appears, provided that the beat frequency between object and reference modulation frequencies is smaller than the inverse response time of the photorefractive crystal (30 Hz for our BSO crystal). If required, we can achieve phase-locking optimization by detecting the conjugate image with a photodetector to generate a feedback signal, which can then be applied either to the photorefractive crystal[11,12] or to the reference-beam modulator.

For moving images, part of the image is left unmodulated and is used as the static portion. The detection of this static portion and the use of the previously described techniques will permit lock-in of the signal, which in turn will permit demultiplexing of the moving image.

It should be stressed that both techniques require that the signal beam laser not jitter appreciably with respect to the object beam laser. As we mentioned above, in our experimental demonstration with static images, this was achieved by using the same laser source and by splitting the beam into object and reference legs.

## Conclusions

An optical demodulation technique has been demonstrated that utilizes the low-bandpass characteristics of a photorefractive material. We have experimentally demultiplexed actual images with (subkilohertz) carrier frequencies separated by less than 200

Hz, and we have shown that the technique can be extended out to 1-GHz carrier frequencies with similar signal bandwidths.

It should be possible to extend this technique to at least 12 GHz, which is the limit of operation of the $LiTaO_3$ modulators.[13] Because currently some ferroelectric crystals can angularly multiplex a few hundred holograms, we expect that this technique can multiplex a few hundred gratings.[14]

We thank L. Bouthillette for her help in preparing the figures for this paper. This work was funded in part by the Rome Laboratory Director's Fund.

## References

1. M. Takeda and M. Kitoh, "Spatiotemporal frequency multiplex heterodyne interferometry," J. Opt. Soc. Am **9,** 1607–1614 (1992).
2. D. R. Pape, "Acoustoptic signal processors," in *Optical Signal Processing,* J. Horner, ed. (Academic, San Diego, Calif., 1987), chap. 3.3.
3. J. N. Lee, "Optical architectures for temporal signal processing," in *Optical Signal Processing,* J. Horner, ed. (Academic, San Diego, Calif., 1987), chap. 3.
4. C. Warde and A. D. Fisher, "Spatial light modulators: applications and functional capabilities," in *Optical Signal Processing,* J. Horner, ed. (Academic, San Diego, Calif., 1987), chap. 7.2.
5. J. Khoury, V. Ryan, C. Woods, and M. Cronin-Golomb, "Photorefractive optical lock in detector," Opt. Lett. **16,** 1442–1444 (1991).
6. J. Khoury, V. Ryan, C. Woods, and M. Cronin-Golomb, "Photorefractive frequency converter and phase sensitivity detector," J. Opt. Soc. Am. B **10,** 72–82 (1993).
7. H. Lee and D. Psaltis, "Photorefractive acoustoelectro-optic correlator," Opt. Lett. **12,** 459–461 (1987).
8. D. Pepper, "Nonlinear optical phase conjugation," Opt. Eng. **21,** 156–183 (1982).
9. J. Khoury, M. Cronin-Golomb, and C. Woods, "Theoretical aspects in frequency division demultiplexing," submitted to Appl. Opt.
10. J. Y. Chang, H. P. Jenssen, and C. Warde, "High photorefractive sensitivity in an N-type-45 cut BaTiO3 crystal," Opt. Lett. **17,** 103–5 (1992).
11. P. N. Ilinykh, O. P. Nestiorkin, and B. Ya. Zeldovich, "Recording of a static hologram in $Bi_{12}TiO_{20}$ by running the interference pattern," in *Conference on Lasers and Electro-Optics,* Vol. 7 of 1990 OSA Technical Digest Series (Optical Society of America, Washington, D.C., 1990), p. 94.
12. T. Sato, T. Hatsuzawa, and O. Ikeda, "Stabilization of BSO phase conjugate using feedback techniques," Appl. Opt. **22,** 1996–1998 (1983).
13. P. A. Shultz and S. R. Henion, "Frequency modulator Nd:YAG laser," Opt. Lett. **16,** 578–580 (1991).
14. F. H. Mok, M. C. Tackitt, and H. M. Stoll, "Storage of 500 high-resolution holograms in a LiNbO3 crystal," Opt. Lett. **8,** 609–611 (1991).

## *MISSION*

## *OF*

## *ROME LABORATORY*

*Rome Laboratory plans and executes an interdisciplinary program in research, development, test, and technology transition in support of Air Force Command, Control, Communications and Intelligence ($C^3I$) activities for all Air Force platforms. It also executes selected acquisition programs in several areas of expertise. Technical and engineering support within areas of competence is provided to ESD Program Offices (POs) and other ESD elements to perform effective acquisition of $C^3I$ systems. In addition, Rome Laboratory's technology supports other AFSC Product Divisions, the Air Force user community, and other DOD and non-DOD agencies. Rome Laboratory maintains technical competence and research programs in areas including, but not limited to, communications, command and control, battle management, intelligence information processing, computational sciences and software producibility, wide area surveillance/sensors, signal processing, solid state sciences, photonics, electromagnetic technology, superconductivity, and electronic reliability/maintainability and testability.*